Biomaterials Science

Design of Apoptotic Cell-Mimetic Wound Dressing using Phosphoserine-Chitosan Hydrogels

Journal:	*Biomaterials Science*
Manuscript ID	BM-ART-07-2023-001259.R1
Article Type:	Paper
Date Submitted by the Author:	28-Sep-2023
Complete List of Authors:	Lee, Gyeongwoo; National Institute for Materials Science, Research Center for Macromolecules and Biomaterials Nabil, Ahmed; National Institute for Materials Science, Research Center for Macromolecules and Biomaterials Kwon, Oh Hyeong; Kumoh Institute of Technology, Department of Polymer Science and Engineering Ebara, Mitsuhiro; National Institute for Materials Science, Research Center for Macromolecules and Biomaterials

ARTICLE

Design of Apoptotic Cell-Mimetic Wound Dressing using Phosphoserine-Chitosan Hydrogels

Received 00th January 20xx,
Accepted 00th January 20xx

DOI: 10.1039/x0xx00000x

Gyeongwoo Lee [a, b], Ahmed Nabil [a, c], Oh Hyeong Kwon [d], and Mitsuhiro Ebara*[a, b, e]

Inflammatory M1 macrophages, creating a hostile environment that impedes wound healing. Phosphoserine (PS) is a naturally occurring immunosuppressive molecule capable of polarizing macrophages from an inflammatory phenotype (M1) to an anti-inflammatory phenotype (M2). In this study, we designed, fabricated, and characterized PS-immobilized chitosan hydrogels as potential wound dressing materials. A PS group precursor was synthesized via a phosphoramidite reaction and subsequently immobilized onto the chitosan chain through an EDC/N-hydroxysuccinimide reaction using a crosslink moiety HPA. The PS/HPA-conjugated chitosan (CS-PS) was successfully synthesized by deprotecting the PS group in HCl. In addition, the hydrogels were prepared by the HRP/H_2O_2 enzyme catalyst reaction with different PS group contents (0, 7.27, 44.28 and 56.88 μmol/g). The immobilization of the PS group improved the hydrophilicity of the hydrogels. Interestingly, CS-PS hydrogel treatment upregulated both pro-inflammatory and anti-inflammatory cytokines. This treatment also resulted in alterations in macrophage cell morphology from the M1 to M2 phenotype. CS-PS hydrogel significantly accelerated diabetic wound healing. Overall, this study provides insights into the potential of PS-immobilized hydrogel materials for improved inflammatory disease therapy.

Introduction

Inflammation control is essential in the wound-healing process. As innate immune cells, macrophages play pivotal roles in inflammation and tissue repairing [1]. They are classified into classically stimulated macrophage (M1) and alternatively stimulated macrophage (M2) [2]. M1 macrophages mediate inflammatory responses, such as reactive oxygen species (ROS) generation, inflammatory cell recruitment, and phagocytosis [3]. Eliminating pathogens and damage-associated molecular patterns stimulates the polarization of M1 macrophages into M2 macrophages, which mediate inflammation resolution, clearance of dead tissues, and tissue repair [4]. Therefore, it is reported that the suppression of inflammation can accelerate the wound healing [5].

Therefore, inflammation control is necessary to realize effective wound healing. Despite the development of numerous anti-inflammatory drugs (e.g., nonsteroidal candidates) and molecular targeted therapies, their therapeutic efficacies remain limited, and they often have drawbacks such as cytotoxicity leading to renal impairment. Common side effects such as stomach ache, nausea, and vomiting, as well as poor bioavailability, further compound their limitations [6,7]. Therefore, new candidates that can effectively control inflammation while minimizing cytotoxicity for improved wound healing are urgently needed. In response to this need, many researchers have recently directed their attention toward oxidative stress suppression as an alternative promising approach to anti-inflammatory therapy. Recently, our research group achieved success in designing and fabricating a hydrogel wound dressing that incorporates catechin, an ROS scavenger. This innovative dressing demonstrated enhanced collagen regeneration while simultaneously inhibiting inflammatory cell recruitment [8]. This result indicates the importance of immune suppression for effective wound healing.

Other trials have focused on direct modulation of the immune microenvironment based on treatment with growth factors and cytokines to improve wound healing. For instance, diabetic mice treated with an optimal concentration of granulocyte-macrophage colony-stimulating factor (GM-CSF) exhibited accelerated wound healing [9]. Other reports have demonstrated that treatments involving platelet-derived growth factor (PDGF) and transforming growth factor beta 1 (TGF-β1) can effectively dampen inflammation and accelerate the wound healing process [10,11]. Interleukin 22 (IL-22) treatment can accelerate wound healing and angiogenesis [12]. This accumulating evidence indicates that modulating immune microenvironments using specific factors, as mentioned above, can be a potent therapeutic approach to achieve improved wound healing. However, due to the complexity of the immune microenvironment in the wounds, except for GM-CSF and PDGF, other cytokine treatments have remained FDA-unapproved [13,14]. Therefore, developing a new therapeutic approach capable of effectively modulating immune

a. Research Center for Macromolecules and Biomaterials, National Institute for Materials Science (NIMS), 1-1 Namiki, Tsukuba 305-0044, Japan
b. Graduate School of Pure and Applied Sciences, University of Tsukuba, 1-1-1 Tennodai, Tsukuba 305-8577, Japan.
c. Biotechnology and Life Sciences Department, Faculty of Postgraduate Studies for Advanced Sciences (PSAS), Beni-Suef University, Beni-Suef 62511, Egypt
d. Department of Polymer Science and Engineering, Kumoh National Institute of Technology, Gumi, Gyeongbuk 39177, Korea† Footnotes relating to the title and/or authors should appear here.
e. Graduate School of Advanced Engineering, Tokyo University of Science, 6-3-1 Katsushika-ku, Niijuku, Tokyo 125-8585, Japan
Electronic Supplementary Information (ESI) available: [details of any supplementary information available should be included here]. See DOI: 10.1039/x0xx00000x

microenvironments for enhanced wound healing is of utmost importance.

Phosphoserine (PS) is a naturally occurring immunosuppressive biomolecule that serves as the lipid head of phospholipids found in the inner cell layer. Interestingly, the PS groups are usually exposed on the cellular surface during apoptosis [15]. Through the uptake of apoptotic cells by various immune cells, exposed PS groups can interact with receptors on these immune cells, resulting in the suppression of immune responses. Exposure to apoptotic cells can trigger macrophage polarization from the M1 to M2 phenotypes [16] and can induce dendritic cell maturation and $CD4^+$ lymphocyte suppression [17,18]. In the previous study, we focused on harnessing the PS immunosuppressive potential by introducing PS groups into a methacrylate polymer chain to fabricate anti-inflammatory nanoparticles. Interestingly, both PS-conjugated synthetic polymer and PS polymer nanoparticles induced significant anti-inflammatory effects. These designed polymers showed diminished pro-inflammatory cytokine secretion while enhancing macrophage polarization from the M1 to M2 phenotypes [19,20].

Despite their immunomodulatory effects, the therapeutic potential of PS remains unclear. Here, we hypothesize that PS stimulates the polarization of macrophage phenotypes, thereby favorably altering the overall immune microenvironment that improves wound healing. To validate our hypothesis, we designed, characterized, and fabricated a PS-immobilized In-situ hydrogel material as a potential immunomodulatory wound dressing (Scheme. 2). Given that 58% of diabetic wounds manifest infections, chitosan was selected for polymer matrix considering inherent anti-microbial activity[21]. The PS groups and crosslink moieties were immobilized onto chitosan polymer while adjusting the degree of PS substitution under varying concentrations. Hydrogels were prepared using the HRP/H_2O_2 enzyme catalyst reaction and evaluated for their gelation time, storage modulus, swelling ratio, biodegradation behavior, and biocompatibility, followed by their anti-inflammatory potential evaluation.

Results and Discussion

Synthesis of PS/HPA-conjugated chitosan

Chitosan was acetylated to improve water solubility and immobilize the PS group. Boc-PS was synthesized using the phosphoramadite reaction, followed by immobilization of Boc-PS and HPA onto the chitosan chain via the EDC/N-hydroxysuccinimide (NHS) reaction. Subsequently, the Boc group was deprotected in HCl to obtain PS/HPA-conjugated chitosan (Scheme 1). To fabricate different PS group contents containing hydrogel, different feed ratios of Boc-PS (0, 5, 50 and 100 w/w%) were used with chitosan (Table S1).

The conjugation of Boc-PS and HPA and the deprotection of the Boc group were characterized using ^{1}H NMR (Fig. 1 a–c). In the acetylated chitosan spectra, only the characteristic peaks of D-glucosamine and N-acetyl glucosamine were observed, except for the solvent peak at 4.9 ppm of water and 2.0 ppm of acetic acid [22]. After conjugation, while the characteristic peaks of the phenol group in HPA were observed at 6.6 and 6.9 ppm, respectively, that of the Boc group was observed at 1.1 ppm. This means that HPA and Boc-PS were simultaneously introduced by the EDC/NHS reaction. After deprotection, while the characteristic peak of the Boc group at 1.1 ppm completely disappeared, those of the phenol group remained. Notably, 4 M HCl seemed to be sufficient to deprotect the Boc group without amide bond cleavage.

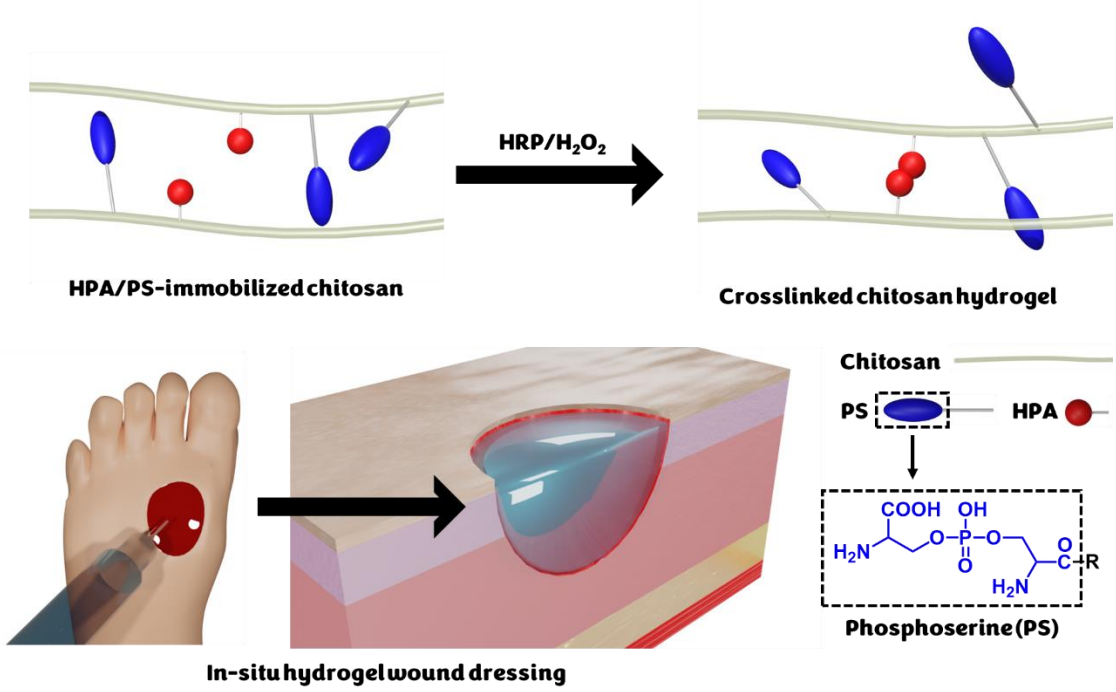

Scheme. 1 Schematic representation of PS/HPA-conjugated chitosan hydrogel and macrophage polarization in the wound.

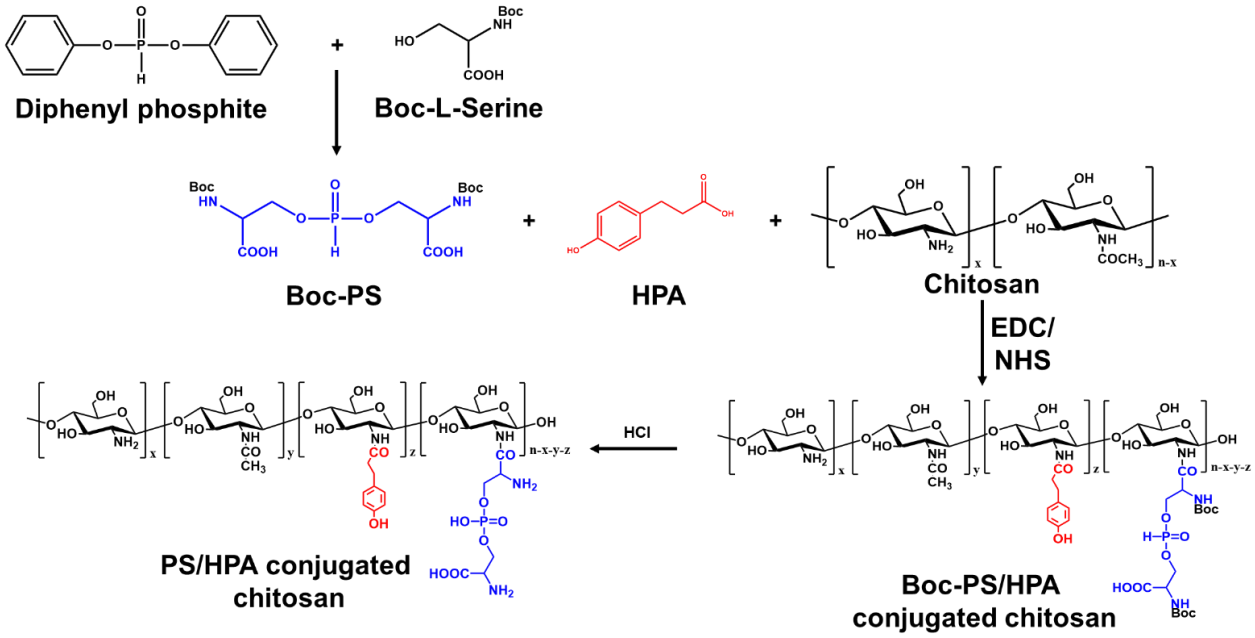

Scheme 2. Synthesis of Boc-PS and conjugation of Boc-PS and HPA to chitosan, and deprotection of the Boc group.

To quantify the PS group, the phosphorous content was quantified by ICP-OES spectroscopy (Fig. 1d). As the PS group contains only one phosphorous molecule, the phosphorous content is equivalent to the PS group content. The phosphorus content of each sample was 1.32, 7.27, 44.28 and 56.88 μmol/g, respectively. The phosphorous content was named to each sample. Neat chitosan was named to CS, and PS incorporated CS was named to the CS-PS 7, CS-PS 44, CS-PS 56 with 5, 50, and 100 w/w% of feed ratio, respectively. Phosphorous content increased with an increase in the feed ratio of Boc-PS, although not a linear increase.

To quantify the HPA group, the phenol group in HPA was quantified by UV–vis spectroscopy. The phenol group contents in each sample were calculated to be 10.4, 9.47, 8.00 and 5.1 μmol/g, respectively. These contents decreased as the Boc-PS feed ratio increased because HPA and Boc-PS competitively reacted to conjugate with the amine group during the EDC/NHS reaction.

Optimization of gelation behavior

The CS and CS-PS was fabricated to hydrogel using the HRP/H_2O_2 enzyme/catalyst reaction (Fig. S1). In this system, HRP acts as a catalyst, and H_2O_2 act as a crosslinking agent. The catalytic cycle of HRP oxidizes the phenol group to phenoxy radicals by converting H_2O_2 to H_2O, after which the oxidized phenoxy radicals can be crosslinked with each other by extinguishing radicals [23].

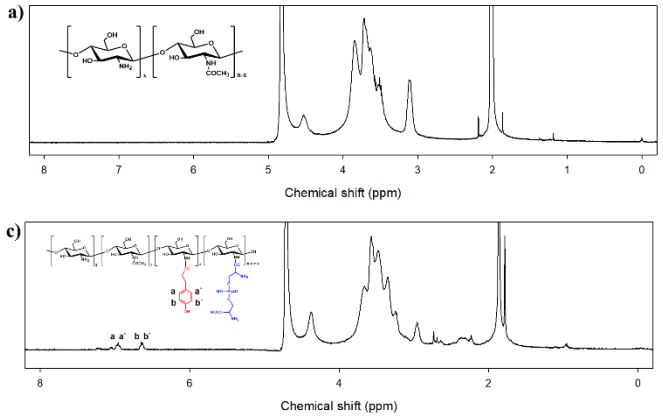

d)

Experimental group	Phosphorous content (μmol/g)	Phenol content (μmol/g)
CS	1.32	10.40
CS-PS 7	7.27	9.47
CS-PS 44	44.28	8.00
CS-PS 56	56.88	5.10

Fig. 1 ^{1}H NMR spectra of the (a) acetylated chitosan, (b) Boc-PS/HPA conjugated chitosan, and (c) after the deprotection. The calculated contents of (d) phosphorous and) phenol in each chitosan derivatives which are measured by ICP-OES and UV-vis spectrometer.

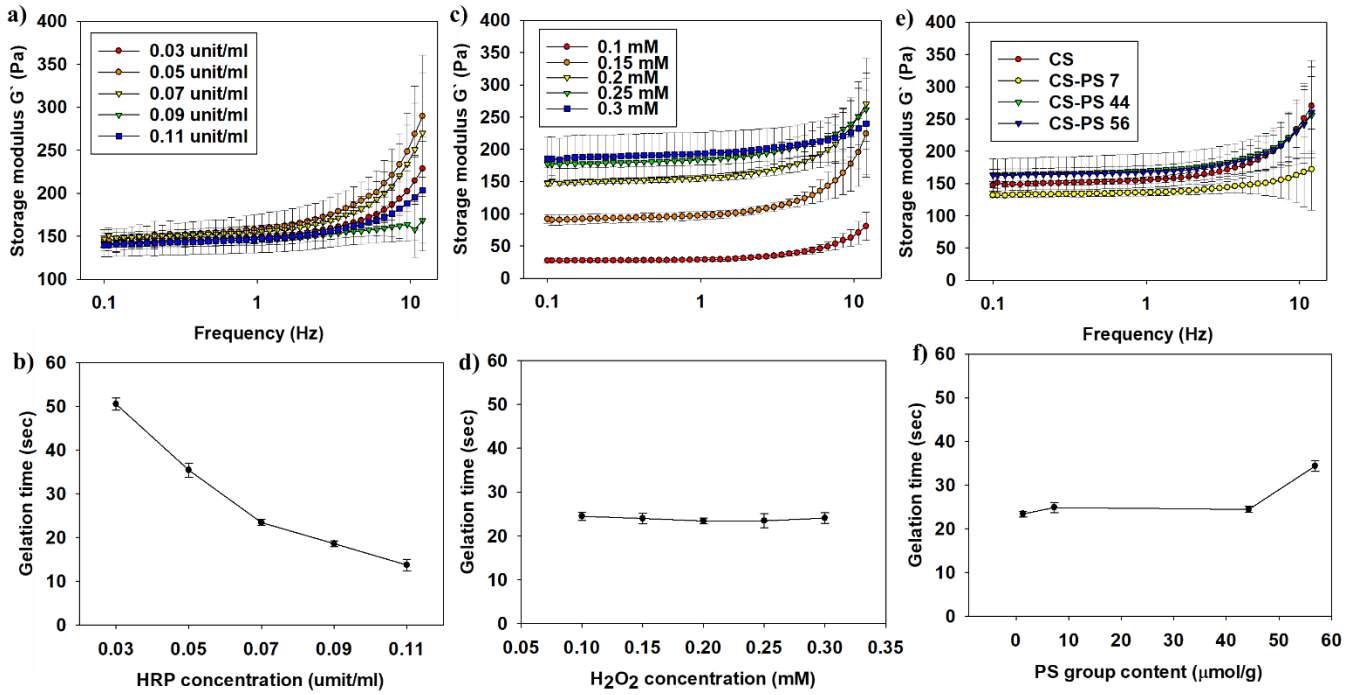

Fig. 2 (a) Storage modulus and (b) gelation time of CS hydrogels upon different HRP concentrations with fixed H_2O_2 concentration at 0.2 mM. (c) Storage modulus and (d) gelation time of CS hydrogels upon different H_2O_2 concentrations with fixed HRP concentration at 0.07 unit/ml. (e) Storage modulus and (f) gelation time of CS and CS-PS hydrogels with fixed HRP and H_2O_2 concentration at 0.07 unit/ml and 0.2 mM, respectively. (Mean ± SD, n = 5).

We measured the storage modulus to optimize the mechanical property and gelation behavior of the hydrogel. The storage modulus and gelation time were measured under different conditions of HRP and H_2O_2 concentrations and Boc-PS feed ratios (Fig. 2). The storage modulus of chitosan hydrogels was not significantly affected by HRP concentrations, but the gelation time was highly decreased from 50 to 14 s following the HRP concentration (Fig. 2a and b). The storage modulus increased from 27 to 185 Pa with the H_2O_2 concentration, but the gelation time was not significantly affected (Fig. 2c and d). These findings corroborated a previous result that showed that excessive H_2O_2 concentrations diminished HRP activity, with decreased a storage modulus [24]. Notably, a decrease in storage modulus was not observed in all H_2O_2 concentrations in this study. Therefore, H_2O_2 did not affect HRP activity during chitosan hydrogel formation, indicating that both the concentration ranges of HRP and H_2O_2 are optimal for stable gelation.

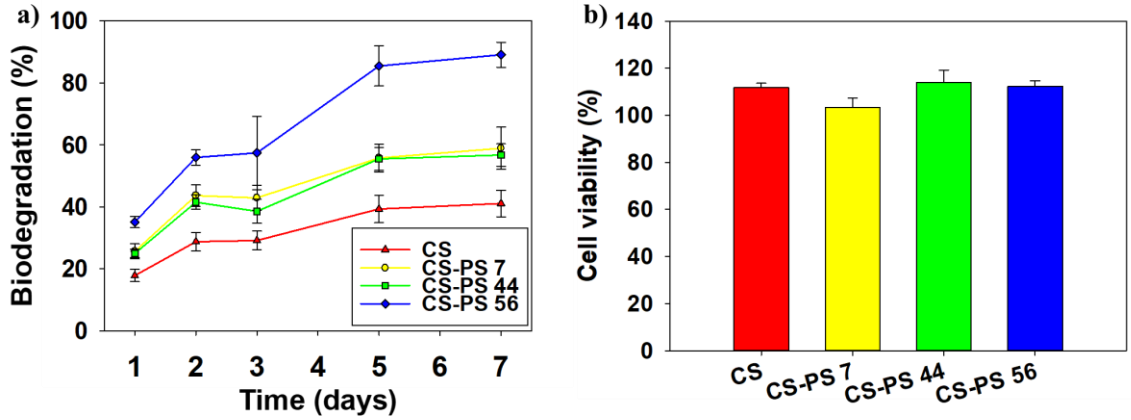

Fig. 3 a) Biodegradation behavior of hydrogels over 7 days in 400 unit/ml of lysozyme containing PBS and b) cell viability of RAW blue™ cell line after coverage with the hydrogel, measured by Alarma blue assay. (Mean ± SD, n = 8).

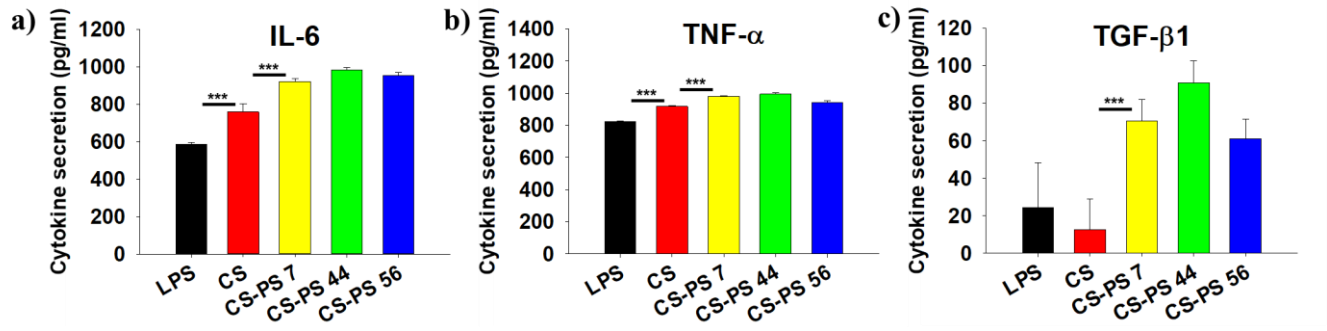

Fig. 4 Cytokine secretion of the pro-inflammatory and anti-inflammatory cytokines: a) IL-6, b) TNF-α, c), and TGF-β1. (Mean ± SD, n = 8, ***: p < 0.001).

The gelation time and storage modulus for the PS group content were tested in the intermediate HRP (0.07 unit) and H_2O_2 (0.2 mM) concentrations (Fig. 2e, f). Regarding the storage modulus, none of the hydrogels showed significant differences between the PS group content. However, the gelation time increased up to 10 s at the highest PS group content. The high feed ratio of the PS group seemed to hinder the substitution of HPA, with low HPA substitution resulting in a delayed gelation time. This data agrees with that of other enzyme/catalyst crosslink hydrogels [25]. An optimal gelation time is important for the usability of an *in situ* gel because crosslinking the gel quickly can trigger nozzle clogging, while prolonged time can result in the hydrogel flowing away from the wound site. The current gelation time range is deemed optimal for convenient applications. The realized storage modulus is considered an optimal range since the human skin has 400 to 1000 Pa of storage modulus [26]. Therefore, this finding suggests that the developed hydrogels do not hinder wound contraction. Notably, we used the current concentrations of HRP and H_2O_2 for continued experiments, as they showed optimized storage modulus and gelation time.

***In vitro* biodegradation and cell viability using the developed hydrogel.**

To test biodegradability, hydrogels were immersed in lysozyme containing PBS with same concentration of wound exudate, and degradation behavior was investigated (Fig. 3a). All hydrogels gradually degraded over 7 days. As the PS group content increased, biodegradability improved. The CS hydrogel showed the slowest biodegradation, while the CS-PS 7 hydrogel showed better biodegradation. The CS-PS 56 hydrogel showed the fastest biodegradation. This result deviates from the relationship with the storage modulus. Biodegradation behavior typically follows mechanical properties because similar mechanical properties mean similar crosslink density [24]. However, despite their similar storage moduli, the hydrogels showed different biodegradation behaviors based on PS group content. Because immobilization of the PS group can yield improved hydrophilicity, thereby accelerating biodegradation, we evaluated hydrophilicity by measuring the equilibrium swelling ratio (Fig. S2). The equilibrium swelling ratio also increased as the PS group content increased. These findings agree with previous reports, which revealed that the immobilization of phosphocholine can improve the hydrophilicity of hyaluronic acid while enhancing material hydration [27]. Also it is reported that enhanced wettability accelerate wound healing by absorption of exudates [28]. Therefore, our data indicates that PS group immobilization improve the hydrophilicity the one of properties for effective wound care.

We evaluated the cell viability of macrophages using the Alamar blue assay after covering them with hydrogels (Fig. 3b). All hydrogel formulations resulted in cell viability exceeding 100%. This means that the chitosan hydrogel itself is nontoxic and that the immobilized PS group can induce biological activity without any cytotoxicity. We also tested the cell viability of fibroblasts (Fig. S3) and found no cytotoxicity, indicating that the non-cytotoxic effect of the fabricated hydrogels is not cell-type specific.

Cytokine secretion and cell morphology

To verify the secretion of cytokines under hydrogel stimulation, cell supernatants were tested by enzyme-linked immunosorbent assay (ELISA) (Fig. 4). Concerning pro-inflammatory cytokines (e.g., TNF-α and IL-6), CS and CS-PS hydrogels induced higher secretion than the control group (Fig. 4a, b), but CS-PS showed higher secretion than CS hydrogel in IL-6 secretion. Despite the increased secretion of pro-inflammatory cytokines, the CS-PS hydrogels also showed improved secretion of TGF-β1 and IL-10 in the case of anti-inflammatory cytokines, which was comparable to that of pro-inflammatory cytokines (Fig. 4c, S4). However, the CS hydrogel did not show significant TGF-β1 secretion but showed similar secretion to the CS-PS hydrogel regarding IL-10. Notably, the effect of the PS group was not concentration dependent.

We believe that this study is the first to immobilize PS groups onto hydrogels in order to evaluate their anti-inflammatory effects. Our findings revealed that the CS-PS hydrogels stimulated macrophages to secrete both IL-10 and TGF-β1 with pro-inflammatory cytokines, while the CS hydrogels showed secretion of only IL-10 and high pro-inflammatory cytokine. Building upon our previous research findings, we discovered that PS-immobilized polymer nanoparticles reduced pro-inflammatory cytokine secretion [19], suggesting chitosan involvement in modulating this secretion.

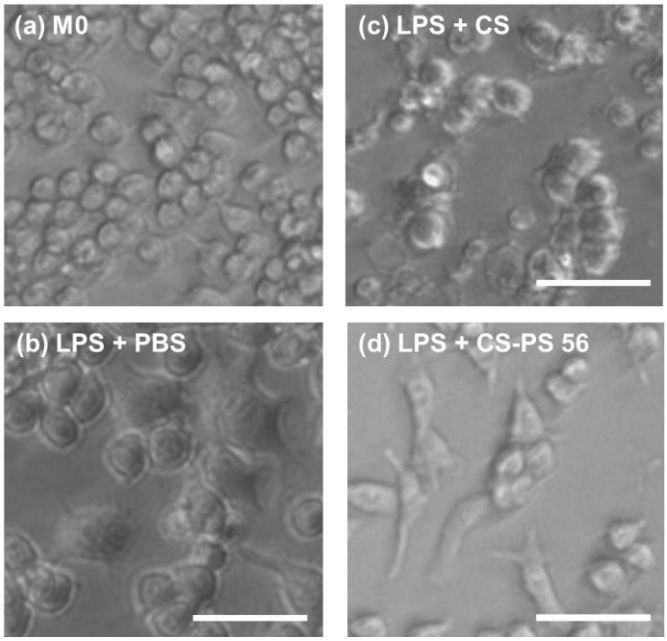

Fig. 5 Optical microscopic image of macrophage (a) before the stimulation and after 24 h of treatment with LPS and (b) PBS, c) CS hydrogel, d) CS-PS hydrogel. (Scale size = 50 μm).

To provide more insight, we reproduced the particle in our previous research, and IL-6 secretion was tested (Fig. S5). The PS group-immobilized nanoparticles showed decreased IL-6 secretion unlike chitosan hydrogels. This data corroborated that of a previous report [29], which revealed that high molecular weight chitosan suppress inflammation, but low molecular weight chitosan promote inflammation. Considering the developed chitosan hydrogels, it is considered that some of low molecular weight chitosan chain was not completely crosslinked and be leaked from hydrogel, and pro-inflammatory secretion was stimulated. Also, this data supports the reason that the effect of PS group doesn't follow concentration dependent manner. In this research, total PS group concentration of particle is 9.3 μM and CS-PS 7 is 35 μM, respectively. It indicates that all PS group concentrations in CS-PS hydrogels are higher than minimum effective dosage.

Macrophages exhibit different cellular shapes depending on their phenotypes. Before LPS stimulation, macrophage (M0) has a circular shape. However, while classically LPS-stimulated macrophage (M1) has a flat and dendrimer-like shape, alternatively polarized macrophage (M2) has a linearly expanded shape [30]. Before and after the sample treatment, the cellular shape of macrophages was observed under an optical microscope (Fig. 5). While M0 macrophage showed a circular shape, macrophages in the control group (LPS and PBS-treated) showed an expanded dendrimer-like shape. The CS hydrogel-treated macrophages also showed an expanded shape compared to M0. Nevertheless, the CS-PS hydrogel-treated macrophages exhibited a linearly extended shape. The PS group in the CS-PS-stimulated macrophage induced macrophagic polarization to an M2 anti-inflammatory phenotype, and these morphological observations corroborated our previous reports [19,20]. Macrophages can be polarized into distinct phenotypes: pro-inflammatory phenotype M1 and anti-inflammatory phenotype M2. However, within the M2 phenotype, specific subsets have been identified, including M2a, M2b, M2c, and M2d. Among these subsets, M2a and M2c macrophages are associated with wound healing and tissue remodeling, while M2b macrophages serve as an immunomodulator between pro-inflammation and anti-inflammation responses. Notably, macrophagic polarization from the M1 to the M2b subset is irreversible. While M2a or M2c macrophages can upregulate the anti-inflammatory cytokines (TGF-β1 and IL-10) and downregulate the pro-inflammatory cytokines (TNF-α and IL-6), M2b macrophages can upregulate both anti-inflammatory and pro-inflammatory cytokines, including IL-10, TNF-α, and IL-6 [31]. The fact that treatment with the CS hydrogel resulted in upregulated levels of IL-6, TNF-α, and IL-10 suggests that this hydrogel polarized macrophages to the M2b subset (Scheme. 2). Because the CS-PS hydrogel upregulated TGF-β1 in addition to the aforementioned, the CS-PS hydrogel-treated

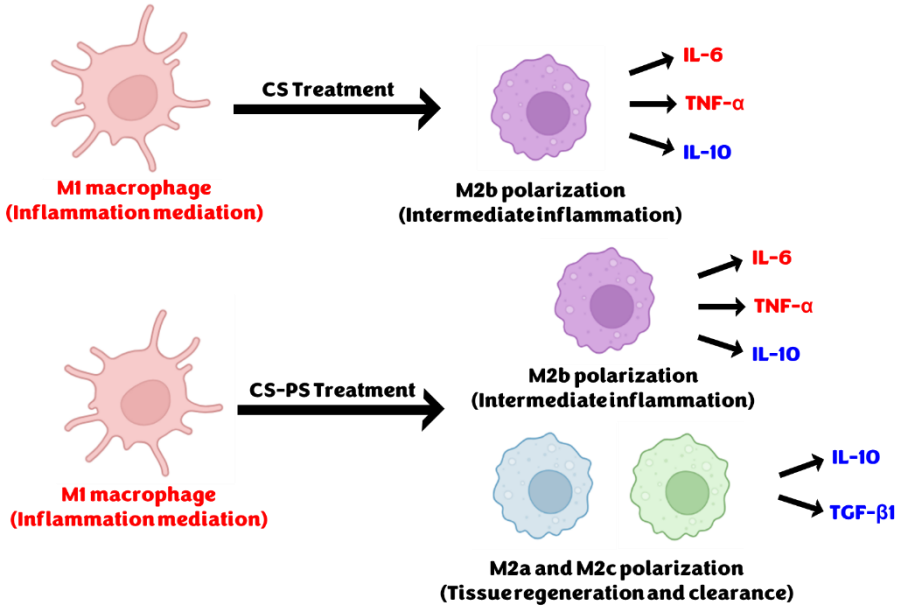

Scheme. 3 Representation of hypothesis to macrophage polarization by chitosan hydrogels treatment.

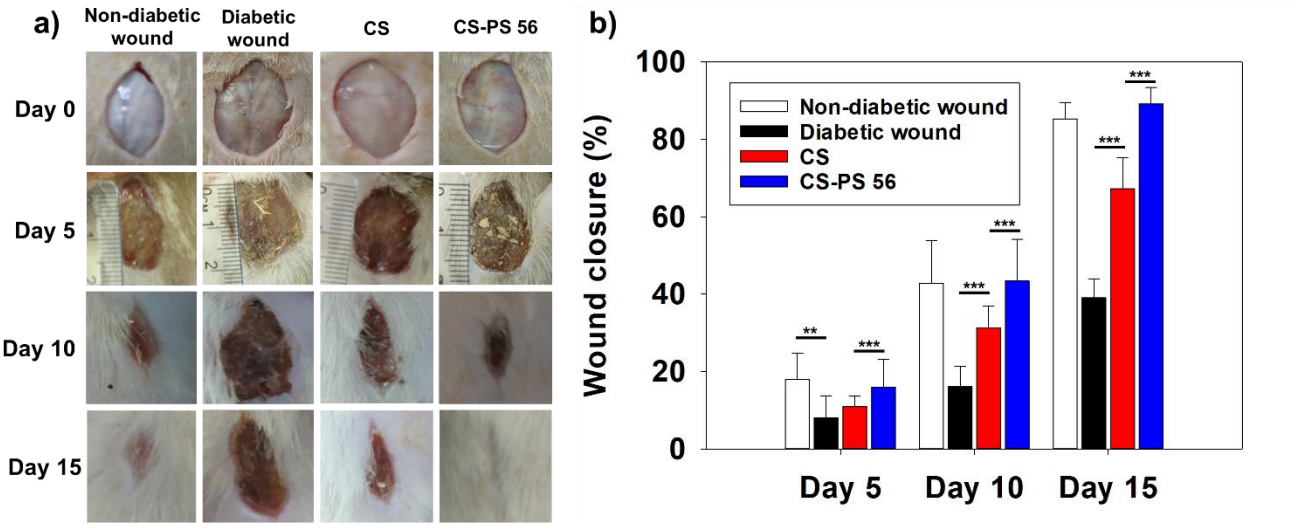

Fig. 6. a) Representative photograph and b) closure profile of full-thickness wound treated by PU film, CS, and CS-PS in diabetic rat animal model. As a negative control, PU film was treated to non-diabetic rat. (Mean ± SD, n=7, **: P<0.01, ***: P<0.001

macrophages are thought to be polarized to all subsets (e.g., M2a, M2b, and M2c). The fact that M2b macrophages were irreversibly polarized to M1 macrophages suggests that constant stimulation under the CS hydrogel can accelerate wound healing by anti-inflammatory macrophages, although it temporarily increases inflammatory cytokines. The CS-PS hydrogel treatment resulted in upregulated levels of TGF-β1, indicating its improved wound healing compared to the CS hydrogel. Especially, it is considered that the chitosan hydrogels will show effective therapeutic effect for diabetic wound. In the case of diabetic wound, constant inflammation environment hinder the wound healing because of the deficiency of immune cells [5,9]. It is reported that GM-CSF treatment increased initial pro-inflammatory cytokine, and immune cell recruited by cytokines. It was led to the improvement of wound healing [9]. In the case of CS-PS hydrogel, it showed increased pro-inflammatory cytokine like GM-CSF. Therefore, it is expected that diabetic wound healing is effectively improved by CS-PS.

Full-thickness diabetic wound healing evaluation

Full-thickness diabetic wound-healing animal model was conducted followed by wound healing ability of CS and CS-PS hydrogels evaluation. Since all CS-PS hydrogel showed similar anti-inflammatory effect, CS-PS 56 was selected for this animal experiment considering hydrophilicity. Type 2 diabetes was successfully conducted in Sprague Dawley rats by Streptozotocin administration as the establishment of this diabetic model was confirmed by measuring blood glucose level (Fig. S6). Wound closure profile was measured at 5, 10, and 15 days after diabetic wound treatment by CS and CS-PS 56 hydrogels, and polyurethane (PU) film dressing was applied on both diabetic and non-diabetic control wound as a negative control and positive control, respectively (Fig. 6). The PU film treated diabetic wound showed retarded wound closure. On the other hand, CS and CS-PS 56 hydrogels showed significantly improved wound closure. Especially, CS-PS 56 hydrogel showed almost equivalent wound closure to the non-diabetic wound.

Hematoxylin & Eosin (H&E) and Masson's trichrome histological staining was considered to evaluate wound healing (Fig. 7a and Fig. S7). Fully covered epidermal layer and repaired dermal layer with skin appendages is observed in non-diabetic wound, while epidermal layer was not fully covered, and granulation tissue was observed in diabetic wound treated by PU film dressing only. Fully covered epidermal layer was observed in CS treated diabetic wound, however skin appendages were not observed. On the other hand, CS-PS 56 treated diabetic wound showed partially repaired skin appendages and improved collagen density than CS treated diabetic wound. The area of granulation tissue was analyzed (Fig. 7b). Granulation in tissues was completely resubstituted to dermal tissue in non-diabetic wound, on the other hand approximately 25, 21.5, and 9.5 mm^2 of granulation tissue was observed in the diabetic wound treated by film, CS, and CS-PS 56, respectively. Total wound healing score was calculated considering wound closure profile and histological analysis (Fig. 7c). In PU film treatment, wound healing scores were 20 in non-diabetic wound and decreased to 7.5 in diabetic wound. CS and CS-PS treated diabetic wound showed score of 13 and 17, respectively.

These results are totally agrees with our hypothesis. Diabetic wound is characterized by deficient macrophage due to hyperglycemia, that leads to impaired wound healing[32]. Therefore, pro-inflammatory cytokine GM-CSF treatment was applied to allow diabetic wound treatment to improve the macrophage recruitment in some reports[9]. In our study, CS treatment improved diabetic wound closure by approximately 200% compared to PU film dressing. According to our *in-vitro* result, CS stimulate pro-inflammatory cytokines and IL-10 secretion (Fig. 4 and Fig. S4). It is considered that macrophages were stimulated to be recruited to the wound lesion by pro-inflammatory cytokines. Afterward, secreted IL-10 inhibited the impaired cytokine secretion of macrophage. In the case of CS-PS 56, TGF-β1 was additionally secreted in the-vitro study. TGF-β1 is cytokine related to the tissue epithelialization and regeneration in wound healing[11]. Secreted TGF-β1 is believed to play an important role in accelerated tissue regeneration, and highly decreased granulation tissue areas, and this also was completely clear in our histological investigations.

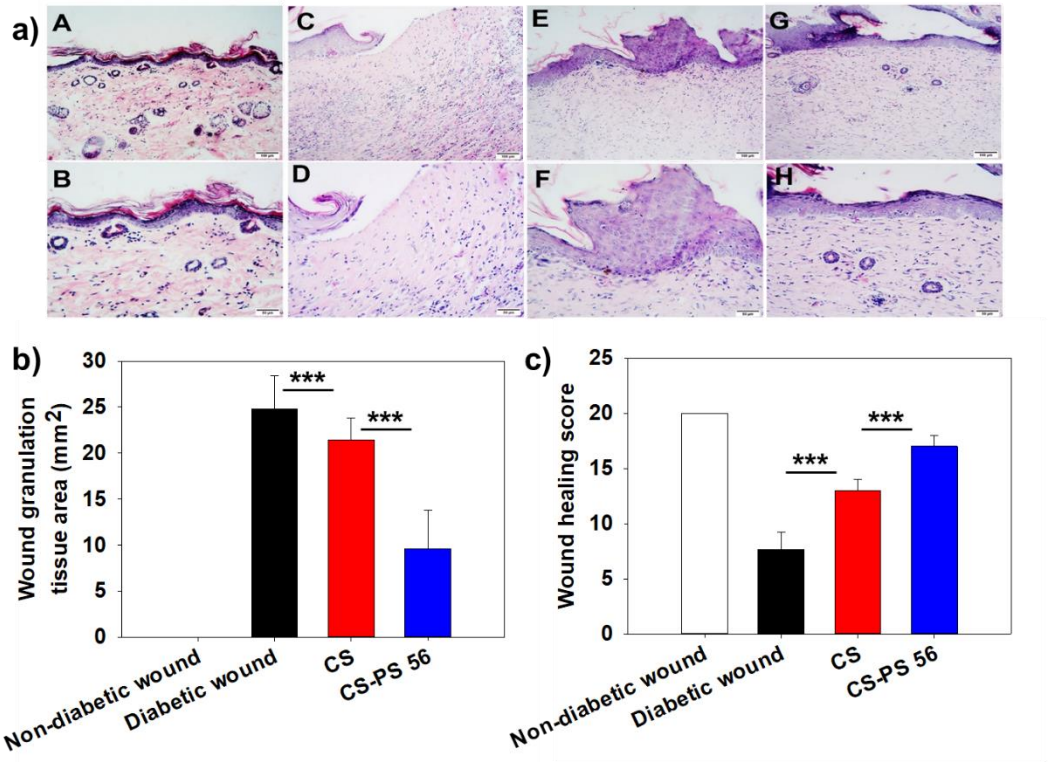

Fig. 7. a) H&E histological photomicgraphs, b) wound granulation tissue area, and c) evaluated wound healing score of wound lesion harvested after 15 days of treatment with PU film, CS, and CS-PS. (A, B: non-diabetic rat treated by PU film; C, D: diabetic rat treated by PU film; E, F: diabetic rat treated by CS; G, H: diabetic rat treated by CS-PS.) (Mean ± SD, n=7, ***: P<0.001)

Cells in wound tissue were stained by IL-6, IL-10, and TGF-β1, and cell populations were investigated to analyze the cytokine secretion profile (Fig. S8). Interestingly, regardless of the type of cytokines, positive cell populations dominantly followed wound healing profile. It is considered that inflammatory cells were decreased, and dermal cells were increased as wound healing. Nonetheless, the anti-inflammatory effect of PS group was observed by population ratio. Comparing PU film and CS, 18% of IL-6 population was decreased while 25% of IL-10 population was decreased. On the other hand, 40% of IL-6 population was decreased while 23% of IL-10 was decreased between CS and CS-PS 56. These results indicate the anti-inflammatory effect of PS 56 group.

It is well known that Chitosan suppresses bacterial growth and improves sensitivity upon antibiotics[33]. Bacteria were collected from each diabetic wound treated with PU film, CS, and CS-PS 56 and incubated on nutrient agar and cystine-lactose-electrolyte-deficient agar (Fig. S9). At days 5 and day 10, bacterial growth was not suppressed by CS and CS-PS 56. On the other hand, bacterial growth was not observed in CS-PS 56 at day 15. It is considered that anti-bacterial effect of chitosan hydrogel is not sufficient, but successful wound healing led to the suppression of bacterial growth. Antibiotics sensitivity against bacterial growth were evaluated bacteria (Table. S3). Some antibiotics showed improved sensitivity upon wounds treated by CS and CS-PS 56 including Cefaclor, Cefatriaxone, Cefamandole, Levofloxacin, Cephalexin, and Vancomycin. This finding is parallel to previous reports[34,35]. Chitosan suppresses bacterial growth through agitation of membrane and suppression of DNA translocation and mitochondrial activity[35,36]. Although a specific mechanism of action is not revealed in this study, it is clear that CS and CS-PS treatment improve the sensitivity of antibiotics. Therefore, incorporating antibiotics in CS and CS-PS hydrogels can improve the effect of anti-biotics and facilitate a topical treatment.

Although CS-PS hydrogel showed excellent cell viability and wound healing ability, it needed to be approved by food and drug administration (FDA) to be commercially available. According to the manual of FDA, medical device is classified into class I, II, and III. Generally, high-class medical device is regarded as hazardous and requires strict screening. General wound dressings without drugs are classified as a class I, and functional wound dressing is classified as a class II or III[37]. According to the decision from FDA in 2016, drug-loaded wound dressing is classified as a class II medical device[38]. Therefore, CS-PS hydrogel is expected to be classified as a class II medical device. For the FDA approval, evidence is important in terms of both safety and therapeutic effect. In this research, the safety of CS-PS hydrogel was proved via ISO-10993 cytotoxicity test and animal experiment. Also, chitosan and PS have been approved by FDA as generally recognized as safe (GRAS) material [39,40]. Therefore, the safety issue is expected to be easily overcame. Since CS-PS showed excellent wound healing ability in animal model, CS-PS hydrogel is expected to be approved by FDA after the therapeutic effect is proved in clinical trials.

Experimental

Materials

For the synthesis part, dimethyl acetamide (anhydrous grade, 99.8%) was purchased from Sigma–Aldrich (USA) and used without any purification. Sigma–Aldrich (USA) also supplied chitosan (low molecular weight, Mw = 50000–190000), acetic anhydride, diphenyl phosphite, pyridine, 2-(N-morpholino)ethanesulfonic acid (MES), 3-(4-hydroxyphenyl)propionic acid (HPA), NHS, horseradish peroxidase (HRP, Type II, 251 unit/mg), lysozyme (recombinant, 100,000 units/mg), and fluorescamine. The Tokyo Chemical Industry (Japan) supplied N-(tert-butoxycarbonyl)-L-serine (Boc-L-serine) and ethyl (dimethylaminopropyl)carbodii*96mide. For macrophage stimulation, lipopolysaccharide (LPS, from *E. coli* K12) was purchased from InvivoGen (France), and recombinant mouse interleukin 4 (IL-4) was purchased from BioLegend (USA). For anti-inflammatory investigations, Alamarblue™ and interleukin 6 (IL-6), tumor necrosis factor α, interleukin 10 (IL-10), and transforming growth factor β1 ELISA, uncoated) kit, IL-10 monoclonal antibody (cat: 11-7101-41) were purchased from Thermo Fisher (USA). IL-6 monoclonal antibody was purchased from Biotechne (USA, cat: AF506). TGF- β1 monoclonal antibody was purchased from Abclonal (USA, cat: A0291).

Synthesis of PS/HPA-conjugated chitosan

Before PS and HPA conjugation to chitosan, we modified chitosan to increase its water solubility using a previously reported method [41]. Briefly, 0.6 g of chitosan was dissolved in 100 ml of 10% acetic acid, and then 2.675 ml of acetic anhydride was added. After 5-h stirring, the solution was neutralized with 5 M NaOH aqueous to pH 7. The neutralized solution was then dialyzed in distilled water for 72 h, with the dialysate being replaced every 24 h. The dialyzed solution was concentrated by rotary evaporator at 40°C. The concentration of the solution was reversely calculated by considering the dried part weight over the solution.

We synthesized Di-boc-L-serine H-phosphonate, the Boc group-deprotected PS (Boc-PS), using a previously reported method [42]. Briefly, 50 mmol of Boc-L-serine was dissolved in 150 ml of DMAc, and 3.75 ml of diphenyl phosphite and 20 ml of pyridine were added. After 24-h stirring under a nitrogen atmosphere, DMAc and pyridine were removed using a rotary evaporator at 50°C. After synthesis, Boc-PS was immobilized with HPA simultaneously using the EDC/NHS reaction. Briefly, a water-solubilized chitosan solution was prepared, and the pH was adjusted to 6. EDC, NHS, and HPA were dissolved in the chitosan solution at 10, 2.5, and 0.5 mg/ml, respectively. Afterward, Boc-PS was added at various concentrations of 0, 0.5, 5, and 10 mg/ml, respectively. After 12-h stirring, the solution was dialyzed in 100 mM NaCl aqueous and deionized water for 48 h, respectively. The dialysate was then replaced every 24 h. After dialysis, the solution was concentrated by rotary evaporator at 40°C.

Finally, to deprotect the Boc group (tert-butoxycarbonyl group) in immobilized Boc-PS, 35% HCl was added to the concentrated solution to reach a chitosan final concentration of 0.5 w/w% and 4 N of HCl. After 2-h stirring, the solution was neutralized to pH 7, followed by 72-h dialysis, with the dialysate being replaced every 24 h. The dialyzed solution was concentrated by rotary evaporator at 40°C. A small portion of the solution was dried over, and the concentration of solution was calculated.

Synthetic material characterization

We verified Boc-PS synthesis, PS–HPA immobilization, and Boc group deprotection using proton nuclear magnetic resonance (^{1}H NMR, Bruker Biospin Advance III, Germany). All samples were dissolved in 1 w/v% acetic acid-d6 (in deuterium oxide) at a concentration of 1 mg/ml for ^{1}H NMR measurements. To calculate the synthesis rate of Boc-PS, the integrated intensities of characteristic peaks of proton in the diphenyl phosphite (7.12–7.2 ppm) and phenol groups (7.2–7.3 ppm) were compared. The immobilization of HPA was confirmed by observing the characteristic peak of the phenol group (7.0–7.4 ppm). The immobilization and deprotection of Boc-PS were confirmed by observing the characteristic peak of the Boc group (1.1 ppm).

We quantified the phosphorous content in the modified chitosan using inductively coupled plasma optical emission spectroscopy (ICP-OES, ES-720, Varian, USA). The modified chitosan was dissolved in water, after which the samples were diluted and measured. The phosphorous characteristic peak at 178.284 nm was observed, and its concentration was calculated by comparing it with the phosphorous standard curve.

The phenol group content in the modified chitosan was quantified using UV–visible spectroscopy (UV–vis; V-650 spectrophotometer, Jasco, Japan). The modified chitosan was dissolved in water at a concentration of 250 µg/ml and measured. The characteristic peak of the phenol group was observed at 274 nm, and its concentration was calculated by comparing the HPA standard curve.

Fabrication and evaluation of PS/HPA-conjugated chitosan hydrogel

We fabricated the hydrogel using the enzyme/catalyst reaction [25]. Briefly, the condensed chitosan solution, 10X PBS, HRP, and distilled water were added to a tube and vortexed. After that, H_2O_2 was added to the tube and vortexed. The final concentrations of the polymer, PBS, HRP, and H_2O_2 were 0.5 w/w%, 1X, 0.07 unit/ml, and 0.2 mM, respectively. After gelation, the hydrogels were incubated in a humid chamber at 37°C for 15 min to be fully crosslinked.

The storage modulus and gelation time were measured to determine the optimal composition of the hydrogel. The storage modulus (G`) was measured between the parallel plate (20 mm) of a rotational rheometer (ARES, TA instrument, USA) with a gap of 1.5 mm for the frequency sweep test. Its values between 0.1 and 12 Hz were measured at 25°C. Through the vial tilting method, the gelation time was measured. Briefly, 0.5 g of pre-gel solution was prepared in a 1.5-mL centrifuge tube. After 2-s vortexing, the tube was tilted every second. As the pre-gel solution stopped flowing, time was recorded.

To evaluate their biodegradation properties, the hydrogels were fabricated in a cylindrical shape measuring 20 mm in diameter and 1.5 mm in height. We immersed the fabricated hydrogel in 5 ml of lysozyme containing PBS at 400 unit/ml. To quantify hydrogel degradation, the amine group content in the hydrogel supernatant was analyzed by fluorescamine assay. Supernatants were collected at 1, 2, 3, 5, and 7 days, after which the biodegradation rate was calculated through amine group quantification.

Macrophage cell culture and stimulation conditions

The mouse macrophage cell line Raw blue™ (Invitrogen, USA) was cultured in Dulbecco's modified Eagle medium (DMEM; Nacalai, USA) supplemented with 10% fetal bovine serum (Sigma–Aldrich, USA) and 1% penicillin-streptomycin (Sigma–Aldrich, USA) under 5% CO_2 at 37°C. To test the cell viability and anti-inflammatory properties of the hydrogel, the cells were seeded at a density of 10^5 cells/well and incubated for 24 h to attach to the plate. After 24 h, 4 µg/ml of LPS containing PBS was added as 10 µl to the each well. After 30 min, the medium was aspirated, followed by PBS washes of the cells, and 30 µl of hydrogels were crosslinked onto the cells and incubated for 15 min to ensure complete crosslinking. Next, 150 µl of medium was added, and the cells were re-incubated for 24 h. The cellular morphology was observed using a phase-contrast microscope (ECLIPSE Ti2; Nikon, Japan). After that, cells and cell supernatants were collected for further investigations.

Cell viability assay and cytokine investigations

Cell viability was evaluated by the Alamar blue assay. Briefly, the Alamar blue stock solution was diluted 11 times with DMEM. After the cell stimulation with LPS, 110 µl of Alarma blue working solution was added to each well. After 3 h, the absorbance of each well was observed using a plate reader (Infinite® 200 PRO, Tecan, Switzerland) at 570 nm under 600 nm of reference.

Cytokine secretions were quantified by ELISA following the manufacturer's instructions. To quantify pro-inflammatory cytokines, TNF-α and IL-6 levels were measured. For anti-inflammatory cytokine quantification, TGF-β1 and IL-10 levels were measured. The cell supernatants were collected after LPS stimulation and analyzed using an ELISA kit following the manufacturer's instructions.

In-vivo full-thickness diabetic wound healing animal model

The diabetic Rats were induced by streptozotocin (STZ). Briefly, to induce diabetic Mellitus-like symptoms, 28 male Sprague Dawely Rats (Weight: 200-250 gm) were purchased from Medical Experimental Research Center (MERC), faculty of medicine, Mansoura University, Egypt and maintained under standard housing conditions (temperature 18–24°C; relative humidity 45–60%; 12: 12 h daylight/darkness). Food and water were provided ad libitum. All animals were treated according to the Guide for the Care and Use of Laboratory Animals published by the US National Institute of Health (Publication No. 85–23, revised 1996). Ethical rules relating to laboratory animals' trials and treatment were agreed upon and followed under Egyptian Liver Research Institute and Hospital (ELRIAH) Experimental Animals Ethical Committee (No. AR2023/057). Rats were randomly divided and injected with STZ intraperitoneally (50 mg/kg body weight), and wound was introduced with 1.5 cm of diameter after 4 days. CS and CS-PS 56 was applied on the diabetic wound, and PU film dressing was applied on the non-diabetic and diabetic wound as a negative control and positive control, respectively. Glucose level was measured using Accu-Check Performa glucose meters (Roche Diabetes Care Limited, United Kingdom), and photograph was recorded at day 0, 5, 10, and 15. Wound closure was calculated with following equation.

$$Wound\ closure\ (\%) = [A0 - At]/A0 \times 100$$

where A0 is the initial wound area and at is the wound area at the same time interval of "t" days[43].

At the end of the experiment, rats from each group were euthanized by decapitation under general anesthesia with thiopental, and wound tissues were collected. All specimens were formalin-fixed, paraffin-embedded and cut into 10 µm-thick sections, which were mounted onto glass slides. These slides were placed in a metal staining rack and immersed in the filtered Harris Hematoxylin for 10 seconds and in EOSIN stain for ~30 seconds[44,45]. For the Masson's trichrome staining, H&E stained slides were immersed in Biebrich Scarlet-Acid Fuchsin solution for 5 minutes, 1% Phosphomolybdic acid solution for 2 minutes, Aniline Blue solution for 5 minutes and Acetic acid solution for 30 seconds [46]. Then, the slides were dehydrated in ascending alcohol solutions and cleared with xylene. Coverslips were mounted onto the sections on the slides with Permount and observed with optical miscroscope**.** The mean wound granulation tissue area measured in 3 non-overlapping fields measured using was measured according to Gal. et al[47]. According to Sultana et al[48] utilized scoring of 6 histological parameters to give a healing score that is amount of granulation tissue (profound-1, moderate-2, scanty-3, absent-4), inflammatory infiltrate (plenty 1, moderate 2, a few 3) collagen fiber orientation (vertical 1, mixed 2, horizontal 3) pattern of collagen (reticular-1, mixed-2, fascicle-3) amount of early collagen (profound-1, moderate-2, minimal-3, absent-4) amount of mature collagen (profound-1, moderate-2, minimal-3) The total healing score in each case was calculated by adding the scores of individual criteria, with lower scores indicating poorer wound healing. Healing status was graded as good (16-19), fair (12-15) and poor (8-11).

For the flow cytometry evaluation, the skin tissues were rinsed with PBS. Then, the tissues were minced with a blade, and an enzymatic dissociation was carried out by introducing a digestion cocktail to minced tissues and incubated at 37°c. Following enzymatic dissociation, the suspension was filtered in order to exclude any undigested tissue pieces from the newly prepared single cell suspension[49]. 50 µl of cell suspension was added to a reagent tube, then 10 µl of conjugated IL-6, IL-10, and TGF-β1 monoclonal antibody was added. The tube was vortexed and incubated for 15 min at room temperature in the dark. The cell suspension was centrifuged for 2 minutes at 828g and the supernatant was removed and dispensed in 200 µl of PBS. Then, the cell suspension was analyzed by flow cytometry[50–52].

A wound swaps were used to transport microorganisms. A squiggly line was drawn lightly on the agar, and petri dish was incubator at 37 °C for 24 hours. Next, disks of filter paper, each impregnated with a standard concentration of an antibiotic, were applied to the plate surface. Antibiotic susceptibility was evaluated via bacterial growth area and inhibition zone was evaluated.

Statistical analysis

Data were expressed as means ± standard deviation, unless otherwise stated. Statistical comparison was performed by one-way ANOVA with Tukey's multiple comparison test using Sigma plot 13 software (Systat software, USA). A p-value of less than 0.05 was considered statistically significant.

Conclusion

We successfully introduced the PS group and HPA to the chitosan chain using the EDC/NHS reaction, as confirmed by NMR and ICP-OES analyses. The resulting CS and CS-PS hydrogels exhibited desirable storage modulus and gelation behavior. The incorporation

of the PS group improved hydrogel hydrophilicity without causing adverse effects or cellular cytotoxicity. Treatment with the CS-PS hydrogel stimulated macrophages to secrete anti-inflammatory cytokines and promoted their polarization to the M2 anti-inflammatory phenotype, and it led to the improvement of therapeutic effect. Overall, the modification with the PS groups not only improved the hydrophilicity but also enhanced immunosuppressive properties of our material, suggesting its potential for various biomedical applications.

Author Contributions

G. Lee and M. Ebara designed the research. K. Oh Hyeong provided reagents for research. G. Lee and A. Nabil performed the research. G. Lee, A. Nabil, O. H. Kown, and M. Ebara analyzed the data. G. Lee, A. Nabil and M. Ebara designed the figures and wrote the text. G. Lee, A. Nabil and M. Ebara analyzed and discussed the data. All authors have read and agreed to the published version of the manuscript.

Conflicts of Interest

The authors declare that they have no conflicts of interest.

Acknowledgments

The research was supported by the JSPS KAKENHI Grant-in-Aid for Scientific Research (B) (JP19H04476) and the Grant-in-Aid for Transformative Research Areas (A) (JP20H05877). Also, this work was supported by JST, the establishment of university fellowships toward the creation of science technology innovation, Grant Number JPMJFS2106.

Notes and References

1 Y. Mo, H. Sarojini, R. Wan, Q. Zhang, J. Wang, S. Eichenberger, G. J. Kotwal and S. Chien, *Frontiers in Pharmacology*, 2020, **10**, 1–14.
2 N. X. Landén, D. Li and M. Ståhle, *Cellular and Molecular Life Sciences*, 2016, **73**, 3861–3885.
3 P. Krzyszczyk, R. Schloss, A. Palmer and F. Berthiaume, *Frontiers in Physiology*, 2018, **9**, 1–22.
4 J. N. Fullerton and D. W. Gilroy, *Nature Reviews Drug Discovery*, 2016, **15**, 551–567.
5 D. V. Verdolino, H. A. Thomason, A. Fotticchia and S. Cartmell, *Emerging Topics in Life Sciences*, 2021, **5**, 523–537.
6 E. Duchesne, S. S. Dufresne and N. A. Dumont, *Physical Therapy*, 2017, **97**, 807–817.
7 K. H. Katsanos and K. A. Papadakis, *Gut and Liver*, 2017, **11**, 455–463.
8 G. Lee, Y. G. Ko, K. H. Bae, M. Kurisawa, O. K. Kwon and O. H. Kwon, *Biomaterials Research*, 2022, **26**, 1–16.
9 Y. Fang, J. Shen, M. Yao, K. W. Beagley, B. D. Hambly and S. Bao, *British Journal of Dermatology*, 2010, **162**, 478–486.
10 I. V. Maggay, A. Venault, C. Y. Fang, C. C. Yang, C. H. Hsu, C. Y. Chou, K. Ishihara and Y. Chang, *ACS Biomaterials Science and Engineering*, 2021, **7**, 562–576.
11 H. El Gazaerly, D. M. Elbardisey and H. M. Eltokhy, *International Journal of Health Sciences*, 2013, **7**, 160–172.
12 S. Avitabile, T. Odorisio, S. Madonna, S. Eyerich, L. Guerra, K. Eyerich, G. Zambruno, A. Cavani and F. Cianfarani, *Journal of Investigative Dermatology*, 2015, **135**, 2862–2870.
13 S. Barrientos, H. Brem, O. Stojadinovic and M. Tomic-Canic, *Wound repair and regeneration*, 2014, **22**, 569–578.
14 M. Bowlby, P. Blume, B. Schmidt and R. Donegan, *Chronic Wound Care Management and Research*, 2014, 11.
15 Y. S. Wu and S. N. Chen, *Frontiers in Pharmacology*, 2014, **5 JAN**, 1–6.
16 V. A. Fadok, D. L. Bratton, S. C. Frasch, M. L. Warner and P. M. Henson, *Cell Death and Differentiation*, 1998, **5**, 551–562.
17 X. Chen, K. Doffek, S. L. Sugg and J. Shilyansky, *The Journal of Immunology*, 2004, **173**, 2985–2994.
18 R. Wang, M. Hao, X. Kou, B. Sui, M. L. Sanmillan, X. Zhang, D. Liu, J. Tian, W. Yu, C. Chen, R. Yang, L. Sun, Y. Liu, C. Giraudo, D. A. Rao, N. Shen and S. Shi, *Bioactive Materials*, 2022, **25**, 472–484.
19 Y. Nakagawa, A. Saitou, T. Aoyagi, M. Naito and M. Ebara, *ACS Macro Letters*, 2017, **6**, 1020–1024.
20 Y. Nakagawa, Y. Yano, J. Lee, Y. Anraku, M. Nakakido, K. Tsumoto, H. Cabral and M. Ebara, *ACS Biomaterials Science and Engineering*, 2019, **5**, 5705–5713.
21 S. R. Nussbaum, M. J. Carter, C. E. Fife, J. DaVanzo, R. Haught, M. Nusgart and D. Cartwright, *Value in health : the journal of the International Society for Pharmacoeconomics and Outcomes Research*, 2018, **21**, 27–32.
22 R. R. L. Vidal, J. Desbrières, R. Borsali and E. Guibal, *Separation Science and Technology (Philadelphia)*, 2020, **55**, 835–847.
23 F. Lee, K. H. Bae and M. Kurisawa, *Biomedical Materials (Bristol)*, 2015, **11**, 14101.
24 F. Lee, J. E. Chung and M. Kurisawa, *Soft Matter*, 2008, **4**, 880–887.
25 L. S. Wang, C. Du, J. E. Chung and M. Kurisawa, *Acta Biomaterialia*, 2012, **8**, 1826–1837.
26 B. Holt, A. Tripathi and J. Morgan, *Journal of Biomechanics*, 2008, **41**, 2689–2695.
27 Y. Zheng, J. Yang, J. Liang, X. Xu, W. Cui, L. Deng and H. Zhang, *Biomacromolecules*, 2019, **20**, 4135–4142.
28 L. Liu, H. Sun, J. Zhang, B. Xu, Y. Gao, D. Qi, Z. Mao and J. Wu, *Advanced Fiber Materials*, 2023, **5**, 574–587.
29 S. H. Chang, Y. Y. Lin, G. J. Wu, C. H. Huang and G. J. Tsai, *International Journal of Biological Macromolecules*, 2019, **131**, 167–175.

30 F. Y. McWhorter, T. Wang, P. Nguyen, T. Chung and W. F. Liu, *Proceedings of the National Academy of Sciences of the United States of America*, 2013, **110**, 17253–17258.
31 L. xun Wang, S. xi Zhang, H. juan Wu, X. lu Rong and J. Guo, *Journal of Leukocyte Biology*, 2019, **106**, 345–358.
32 K. Moore, F. Ruge and K. G. Harding, *The British journal of dermatology*, 1997, **137**, 188–194.
33 M. L. Breser, L. Tisera, M. S. Orellano, L. P. Bohl, P. Isaac, I. Bianco and C. Porporatto, *Frontiers in Microbiology*, 2023, **14**, 1167693.
34 W. N. Kadhum and I. A. Zaidan, *Iraqi Journal of Science*, 2020, **61**, 3187–3199.
35 J. S. Moon, H. K. Kim, H. C. Koo, Y. S. Joo, H. M. Nam, Y. H. Park and M. Il Kang, *Applied microbiology and biotechnology*, 2007, **75**, 989–998.
36 I. Galván Márquez, J. Akuaku, I. Cruz, J. Cheetham, A. Golshani and M. L. Smith, *International journal of food microbiology*, 2013, **164**, 108–112.
37 C. J. Chang and M. Kazemzadeh-Narbat, *Journal of Wound Care*, 2021, **30**, S3–S4.
38 *FDA Executive Summary Classification of Wound Dressings Combined with Drugs Prepared for the Meeting of the General and Plastic Surgery Devices Advisory Panel*, .
39 Office of Food Additive Safety, *GRAS Notice (GRN) No. 997*, College Park, 2021.
40 Office of Food Additive Safety, *GRAS Notice (GRN) No.637*, College Park, 2016.
41 N. Kubota and Y. Eguchi, *Polymer Journal*, 1997, **29**, 123–127.
42 Y. He, X. Wu, G. Zhang, X. Huang, W. Zhang, M. Tu and R. Zeng, *International Journal of Biological Macromolecules*, 2020, **163**, 1738–1746.
43 N. M. Mahajan, K. Wanaskar, N. Ali, D. K. Mahapatra, M. Iqbal, A. R. Bhat and M. Kaleem, *Gels*, 2023, **9**, 462.
44 S. Thompson, *Selected histochemical and histopathological methods*, IL, Springfield, 1966.
45 B. H. Sheehan, DC, *Theory and practice of histotechnology*, OH, Columbus, 2nd edn., 1987.
46 H. Abe, K. Kamimura, Y. Kobayashi, M. Ohtsuka, H. Miura, R. Ohashi, T. Yokoo, T. Kanefuji, T. Suda, M. Tsuchida, Y. Aoyagi, G. Zhang, D. Liu and S. Terai, *Molecular Therapy - Nucleic Acids*, 2016, **5**, e276.
47 P. Gal, R. Kilik, M. Mokry, B. Vidinsky, T. Vasilenko, S. Mozes, N. Bobrov, Z. Tomori, J. Bober and L. Lenhardt, *Veterinarni Medicina*, 2008, **53**, 652–659.
48 J. Sultana, M. R. Molla, M. Kamal, M. Shahidullah, F. Begum and M. A. Bashar, *Bangladesh Journal of Pathology*, 2009, **24**, 3–8.
49 A. Reichard, K. A.-C. P. A and U. 2019, *Wiley Online LibraryA Reichard, K AsosinghCytometry Part A, 2019•Wiley Online Library*, 2018, **95**, 219–226.
50 I. Çetin, A. Çetin, A. Şen, L. Cimen, B. Çimen, G. Savas, A. Oztürk and M. Y. Koker, *Turkish Journal of Biochemistry*, 2018, **43**, 540–548.
51 M. Kalkal, R. Chauhan, R. Thakur, M. Tiwari, V. P.-Biology and U. 2022, *mdpi.comM Kalkal, R Chauhan, RS Thakur, M Tiwari, V Pande, J DasBiology, 2022•mdpi.com*.
52 M. Niu, M. Yi, Y. Wu, L. Lyu, Q. He, R. Yang, L. Zeng, J. Shi, J. Zhang, P. Zhou, T. Zhang, Q. Mei, Q. Chu and K. Wu, *Journal of hematology & oncology*, 2023, **16**, 94.